Water Research 239 (2023) 119921

Contents lists available at ScienceDirect

Water Research

journal homepage: www.elsevier.com/locate/watres

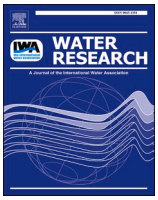

Impact of chlorination and ozonation of dissolved organic matter on its photo-induced production of long-lived photooxidants and excited triplet states

Stephanie C. Remke [a,b], Joanna Houska [a,b], Urs von Gunten [a,b,*], Silvio Canonica [a]

[a] Eawag, Swiss Federal Institute of Aquatic Science and Technology, Überlandstrasse 133, CH-8600 Dübendorf, Switzerland
[b] School of Architecture, Civil and Environmental Engineering (ENAC), Ecole Polytechnique Fédérale de Lausanne (EPFL), CH-1015 Lausanne, Switzerland

ARTICLE INFO

Keywords:
Dissolved organic matter
Ozonation
Chlorination
Long-lived photooxidants
^{3}CDOM*
3,4-dimethoxyphenol

ABSTRACT

Recent studies suggested that long-lived photooxidants (LLPO), which are reactive intermediates formed during irradiation of dissolved organic matter (DOM), may consist of phenoxyl radicals derived from phenolic moieties of the DOM. Besides the well-studied excited triplet states of chromophoric DOM (^{3}CDOM*), LLPO presumably are important photooxidants for the transformation of electron-rich contaminants in surface waters. The main objective of this study was to further test the potential role of phenoxyl radical as LLPO. Suwannee River fulvic acid (SRFA) as a model DOM was pre-oxidised using the phenol-reactive oxidants chlorine and ozone, followed by its characterization by the specific UV absorption at 254 nm ($SUVA_{254}$), the ratio of absorbance at $\lambda = 254$ nm and $\lambda = 365$ nm (E2:E3), and the electron donating capacity (EDC). Subsequently, the photoreactivity of pre-oxidized SRFA was tested using 3,4-dimethoxyphenol (DMOP) as a LLPO probe compound at two initial concentrations ($[DMOP]_0 = 0.1$ and 5.0 μM). Linear inter-correlations were observed for the relative changes in $SUVA_{254}$, E2:E3, and EDC for increasing oxidant doses. Pseudo-first-order transformation rate constants normalized to the changing SRFA absorption rate (i.e., $k^{obs}_{0.1}/r^{abs}_{CDOM}$ and $k^{obs}_{5.0}/r^{abs}_{CDOM}$, for 0.1 and 5.0 μM, respectively) exhibited the following distinct trends: The LLPO-dominated $k^{obs}_{0.1}/r^{abs}_{CDOM}$ ratio decreased with increasing oxidant dose and with decreasing $SUVA_{254}$ and EDC, while the ^{3}CDOM*-dominated $k^{obs}_{5.0}/r^{abs}_{CDOM}$ ratio positively correlated with E2:E3. Finally, it was concluded that precursors of ^{3}CDOM* and LLPO are chemically modified differently by pre-oxidation of DOM, and LLPO precursors likely consist of phenolic moieties of DOM, suggesting phenoxyl radicals as LLPO.

Introduction

Dissolved organic matter (DOM) is ubiquitous in surface waters and describes a complex mixture of organic compounds produced by biogeochemical processes (Leenheer and Croué 2003). DOM spans a broad range of molecular weight, typically between ~100–100,000 Da, and is composed of aliphatic and hydrocarbon structures with various functional moieties, including amides, carbonyls and phenols (Derrien et al., 2019). The chromophoric part of DOM, CDOM, is able to absorb light and consequently to form photochemically produced reactive intermediates (PPRI), which may induce the transformation of micropollutants (Guo et al., 2022; Richard and Canonica 2005; Vione et al., 2014). CDOM-produced PPRI include short-lived photooxidants, such as the pool of excited triplet states of the CDOM, ^{3}CDOM* (McNeill and Canonica 2016). Furthermore, long-lived photooxidants (LLPO) form upon CDOM light absorption and have been observed to enhance ^{3}CDOM*-induced transformation processes (Canonica and Freiburghaus 2001; Canonica and Hoigné 1995; Kawaguchi 1993; Remke et al., 2021). LLPO have estimated lifetimes of ~100 μs and were found to be relevant for the transformation of electron-rich, (i.e. readily oxidizable), phenols, phenylureas and anilines (Canonica and Hoigné 1995; Remke et al., 2021). It has been hypothesized that LLPO precursors are phenolic moieties of DOM (Buschmann et al., 2005; Remke et al., 2021). Moreover, photochemically produced phenoxyl radicals were successfully used to mimic the enhancement effect ascribed to LLPO (Remke et al., 2022; Remke et al., 2021).

For the assessment of CDOM-induced photochemistry, probe compounds are commonly employed to identify and/or quantify PPRI

* Corresponding author at: Eawag, Swiss Federal Institute of Aquatic Science and Technology, Überlandstrasse 133, CH-8600 Dübendorf, Switzerland.
E-mail address: urs.vongunten@eawag.ch (U. von Gunten).

https://doi.org/10.1016/j.watres.2023.119921
Received 21 September 2022; Received in revised form 19 March 2023; Accepted 26 March 2023
Available online 30 March 2023

(Rosario-Ortiz and Canonica 2016). To measure ^{3}CDOM*-induced oxidations, mostly 2,4,6-trimethylphenol (TMP) was used as a probe compound (Berg et al., 2019; Bodhipaksha et al., 2015; McNeill and Canonica 2016). A further parameter used to describe the efficiency of TMP-reactive ^{3}CDOM* formation for a given DOM is the quantum yield coefficient, f_{TMP}, defined by eq. (1) as the pseudo-first-order phototransformation rate constant of TMP, k^{obs}_{TMP} (s^{-1}), divided by the rate of light absorption by CDOM, r^{abs}_{CDOM}: (moles of photons per liter per second, briefly M s^{-1}):

$$f_{TMP} = \frac{k^{obs}_{TMP}}{r^{abs}_{CDOM}} \quad (M^{-1}) \tag{1}$$

f_{TMP} is proportional to − and used as an indicator of − the intersystem crossing quantum yield (equivalent to the excited triplet formation quantum yield) for TMP-reactive ^{3}CDOM* (Canonica et al. 1995). Previous studies involving chemical reduction of DOM using sodium borohydride and utilizing TMP as a probe compound provided evidence that carbonyl moieties were the main precursors of ^{3}CDOM* (Golanoski et al., 2012; Sharpless 2012).

For the detection of LLPO, mainly 3,4-dimethoxyphenol (DMOP) has been used as a probe compound (Canonica and Freiburghaus 2001; Remke et al., 2021). The quantification of the LLPO effect was based on the determination of the pseudo-first-order rate constants for the phototransformation of DMOP, $k^{obs}_{0.1}$ and $k^{obs}_{5.0}$ at initial DMOP concentrations of 0.1 or 5.0 μM, respectively (Canonica and Freiburghaus 2001; Remke et al., 2021). Two alternative methods for LLPO quantification were used. The first method considered the difference ($k^{obs}_{0.1} - k^{obs}_{5.0}$) to be the minimum contribution of LLPO to k^{obs} at initial DMOP concentration ≤ 0.1 μM (Canonica and Freiburghaus 2001). The second method considered the ratio ($k^{obs}_{0.1}/k^{obs}_{5.0}$), defined as enhancement factor, to the minimum enhancement in k^{obs} due to LLPO with respect to $k^{obs}_{5.0}$, representing the contribution of ^{3}CDOM* to DMOP phototransformation (Remke et al., 2021).

Chemical oxidation of DOM, in particular using chlorination or ozonation, leads to distinct changes in UV absorption spectra, electron donating capacity (EDC) and photochemical reactivity of DOM (Leresche et al., 2021; Önnby et al., 2018; Remucal et al., 2020; Wan et al., 2021; Wenk et al., 2013a; Wenk et al., 2015). Changes in absorption spectra and EDC of DOM are associated to transformations of oxidant-reactive moieties, and linking these changes to photochemical reactivity changes may provide evidence for LLPO precursors. Chlorination and two different types of ozonation in absence and presence of *tert*-butanol (*t*-BuOH), have been used in several of the aforementioned studies and are also employed in the present investigations. Ozonation in the presence of *t*-BuOH is performed to prevent oxidation of DOM through reactions with $^{\bullet}$OH and obtain DOM oxidation exclusively by direct ozone reactions. In contrast, ozonation in absence of *t*-BuOH is characterized by smaller ozone exposures (at equal ozone doses) and less selective modification of various types of DOM moieties as a consequence of $^{\bullet}$OH reactions (Remucal et al., 2020; von Sonntag and von Gunten 2012). Table 1 illustrates the various types of oxidation process and how they affect DOM properties. Note that in this study we focus on three parameters, namely $SUVA_{254}$, E2:E3 and the EDC. $SUVA_{254}$ is an indicator for DOM aromaticity (Weishaar et al., 2003), while E2:E3 is inversely proportional to the DOM molecular weight (Helms et al., 2008; Peuravuori and Pihlaja 1997), i.e., E2:E3 increases with decreasing molecular weight. EDC correlates with the phenolic content of DOM

Table 1
Compilation of observed bulk parameter changes upon DOM oxidation with chlorine and ozone (with/ without *t*-BuOH) and suggested structural changes of DOM (for abbreviations see footnote).

DOM oxidation	Observed parameters	Observation	Suggested reactive sites and mechanism	Suggested structural changes of DOM	Literature
Chlorine	EDC, $SUVA_{254}$	Strong EDC decrease, moderate $SUVA_{254}$ decrease (pH 7)	Oxidation of electron-rich phenol and hydroquinone moieties Chlorination of phenolic moieties	Increase in chlorophenol moieties and benzoquinones	(Önnby et al., 2018; Wenk et al., 2013a)
	TOC, FT-ICR-MS, ^{13}C CP/MAS NMR, CV, EDC, E2:E3	Decrease in EDC, aromaticity and average molecular weight	Electrophilic aromatic substitution of phenolic and aromatic moieties	Formation of quinone-type moieties and chlorinated sites	(Gallard and von Gunten 2002b; Wan et al., 2021)
	UV–vis FT-ICR-MS	Formation of disinfection byproducts	Aromatic moieties are the source for disinfection byproducts	Decrease in aromaticity, fragmentation of DOM	(Milstead and Remucal 2021)
	LC-MS	Detection of formed non-halogenated aromatic intermediates	*β*-diketones, *α*-diol and ester-type moieties are reacting with chlorine and bond cleavage leads to smaller molecules	Fragmentation of DOM	(Jiang et al., 2020)
Ozone (oxidants: O_3 and $^{\bullet}$OH)	EDC, $SUVA_{254}$	Strong EDC decrease, moderate $SUVA_{254}$ decrease (pH 7)	Phenolic moieties are main reactive sites	Decrease in phenolic moieties, formation of benzoquinones	(Wenk et al., 2013b)
	EDC, $SUVA_{254}$, pH variation	EDC and absorbance decrease vary with pH of solution	Phenolic moieties are main reactive sites	pH-dependent transformation of phenolic moieties (high pH more benzoquinone, low pH more ring-opening)	(Önnby et al., 2018)
	EDC, UV–vis, MS	Decrease in aromaticity, apparent molecular weight and EDC	Oxidants react with highly aromatic and reduced formulas and more saturated formulas e.g. by addition of oxygen atom (s) and/or decarboxylation	Highly oxidized DOM is formed (O:C > 1) Due to the presence of $^{\bullet}$OH also transformation of saturated formulas	(Remucal et al., 2020)
Ozone in presence of *t*-BuOH (oxidant: O_3)	EDC, $SUVA_{254}$	Strong EDC decrease, moderate $SUVA_{254}$ decrease (pH 7, similar to experiments without *t*-BuOH)	Electrophilic addition to aromatic moieties, followed by ring-cleavage	Decrease in phenolic moieties and activated aromatic sites	(Önnby et al., 2018; Wenk et al., 2013a)
	EDC, UV–vis, MS	Decrease in aromaticity, apparent molecular weight and EDC (larger changes than without *t*-BuOH)	Reaction with aromatic and reduced formulas, e.g. by addition of 1–2 oxygen atoms	Highly oxidized DOM is formed	(Remucal et al., 2020)

EDC: electron donating capacity; $SUVA_{254}$: specific UV absorption coeficient at $\lambda = 254$ nm; TOC: total organic carbon; FT-ICR MS: Fourier transform ion cyclotron mass spectrometry; ^{13}C CP/MAS NMR : ^{13}C cross polarization/magic-angle spinning nuclear magnetic resonance; CV: cyclic voltammetry; E2:E3: ratio of SUVA $\lambda = 254$ nm to $\lambda = 365$ nm; UPLC/ESI-tqMS: ultra performance liquid chromatography/electrospray ionization-triple quadrupole mass spectrometry, Orbitrap mass spectrometry.

(Aeschbacher et al., 2012; Houska et al., 2021; Önnby et al., 2018; Walpen et al., 2016). Phenolic moieties and hydroquinones are major reactants for oxidants (Gallard and von Gunten 2002a; Önnby et al., 2018; Wenk et al., 2013a). Moreover, chlorination leads to the formation of e.g. chlorophenols (Gallard and von Gunten 2002b), while ozonation, besides benzoquinone, also leads to the formation of aliphatic ring opening products (Mvula and von Sonntag 2003; Ramseier and von Gunten 2009).

This study tests the hypothesis that LLPO precursors are phenolic DOM moieties and evaluates the relationship between changes in photoreactivity and changes in characteristic DOM parameters, i.e., $SUVA_{254}$, E2:E3 and EDC. In this study, Suwannee River fulvic acid (SRFA) was employed as a model DOM and changes in the aforementioned parameters of SRFA upon oxidation with chlorine and ozone (the latter performed in buffered aqueous solutions at pH 7 with or without *t*-BuOH) were evaluated. Subsequently, the oxidized SRFA was inspected for changes in pseudo-first-order phototransformation rate constants of DMOP (initial concentrations of 0.1 and 5.0 μM). Finally, changes in $SUVA_{254}$, E2:E3 and EDC were correlated to the changes in pseudo-first-order rate constants for the transformation of DMOP photosensitized by pre-oxidized SRFA.

Material and methods

2.1. Chemicals and solutions

The following chemicals were obtained from commercial sources and used as received: 3,4-dimethoxyphenol (DMOP; Alfa Aesar, 98%), $Na_2HPO_4{\cdot}2H_2O$ (Sigma Aldrich/Merck, ≥98.5%) and $NaH_2PO_4{\cdot}H_2O$ (Merck, for analysis) and the DOM isolate Suwannee River fulvic acid (SRFA, type "standard III", 3S101F, International Humic Substances Society, IHSS).

Ultrapure water with a resistivity of >18.2 MΩ•cm was obtained from an Arium® pro ultrapure water system (Sartorius AG, Goettingen, Germany). Stock solutions of 3,4-dimethoxyphenol (10 or 500 μM) were prepared in ultrapure water. Phosphate buffer stock solutions (50 mM, pH 7.76 and 100 mM, pH 6.7) were prepared in ultrapure water by dissolving appropriate amounts of $Na_2HPO_4{\cdot}2H_2O$ and $NaH_2PO_4{\cdot}H_2O$. SRFA stock solutions (≈ 60 $mg_C L^{-1}$) were prepared in ultrapure water by dissolving an estimated target amount of the hygroscopic isolates. The concentrations of these SRFA stock solutions were defined by comparison of the measured absorbance at $\lambda = 254$ nm and $\lambda = 365$ nm to aqueous SRFA solution with defined DOC (LOQ = 0.5 $mg_C L^{-1}$, measurement error: 0.2 $mg_C L^{-1}$), measured with a total organic carbon analyzer (TOC-L CSH, Shimadzu, Japan). All solutions were stored in the dark at 4 °C.

2.2. Oxidation of SRFA by chlorine and ozone

SRFA oxidation was performed by mixing oxidant solutions with buffered (phosphate buffer, 10 mM, pH 7) SRFA-containing solutions (10 $mg_C L^{-1}$). Specific oxidant doses of $0 - 0.25$ $mol_{oxidant} \times mol_C^{-1}$ were applied to achieve similar conditions as in a previous study (Wenk et al., 2013a). Ozonation experiments were performed in the absence and presence of 5 mM *t*-BuOH as a scavenger for •OH.

The reaction mixtures were mixed after addition of the oxidants. The solutions were kept at room temperature for 12 h or 2 h for chlorination or ozonation, respectively, and afterwards stored at 4 °C for ≤ a week. UV absorbance and EDC measurements as well as irradiation experiments were performed within 24 h for every batch of oxidized SRFA. The complete workflow is illustrated in Fig. 1.

2.3. Characterization of oxidized SRFA

Before starting the bulk parameter measurements and irradiation experiments, the DPD (APHA 2005) and indigo method (Hoigné and Bader 1980) were employed to detect residual oxidants. For the applied experimental procedure no residual oxidant was detected in any of the samples.

Electron donating capacity (EDC)

The EDC is an operationally defined parameter, which quantifies the moles of electrons transferred from electron donating DOM moieties to a chemical oxidant (Aeschbacher et al., 2012; Walpen et al., 2020). Here, EDC measurements were performed according to the EDC assay from a previous study (Walpen et al., 2020). In brief, this assay uses the radical cation 2,2′-azinobis(3-ethylbenzothiazoline-6-sulfonate) ($ABTS^{\bullet+}$) as a chemical DOM oxidant and the electron-transfer of DOM to $ABTS^{\bullet+}$ to obtain ABTS is measured by a reduction in absorbance at 728 nm (ε = 14′000 M^{-1} cm^{-1}, pH 7.0). Solutions were diluted to DOC concentrations between 0.5 and 3 $mg_C L^{-1}$ to obtain reliable EDC measurements (Walpen et al., 2020).

Absorbance measurements

Absorbance measurements were performed on an Agilent Cary 100 UV–vis spectrophotometer in the double beam mode. Spectra were recorded in the wavelength range of 250–500 nm, and the specific UV absorption at 254 nm ($SUVA_{254}$, units: L mg_C^{-1} m^{-1}) was obtained by dividing the 254 nm absorbance by the cell path length and the concentration of non-oxidized SRFA in terms of mg of carbon. Thereby, it was assumed that the carbon content of SRFA was not significantly affected by pre-oxidation (Wenk et al., 2013a). The E2:E3 was calculated as the ratio of the DOM absorbances at $\lambda = 254$ nm and $\lambda = 365$ nm.

2.4. Steady-state irradiation experiments

Steady-state irradiations were performed in a merry-go-round photoreactor, with the established conditions for the observation of DMOP phototransformation induced by PPRI with differing lifetimes, according to previous publications (Canonica and Freiburghaus 2001; Canonica and Hoigné 1995; Remke et al., 2021). In brief, 16 mL of aqueous solution, containing 2.5 $mg_C L^{-1}$ SRFA (untreated or oxidized), 0.1 or 5.0 μM DMOP, and 5 mM phosphate buffer (pH 8.0) were irradiated in glass-stoppered quartz tubes (18 mm external diameter, 15 mm internal diameter). Seven 360 μL samples were taken in equidistant time intervals (for 0.1 μM every 30 s for 5.0 μM every 2 min). A medium-pressure mercury lamp (Heraeus Noble-light model TQ718, operated at 500 W) served as a light source positioned in a borosilicate cooling jacket with a filter solution (0.15 M sodium nitrate solution, recirculated at 25 °C), resulting in a cut-off filter absorbing light with $\lambda <$

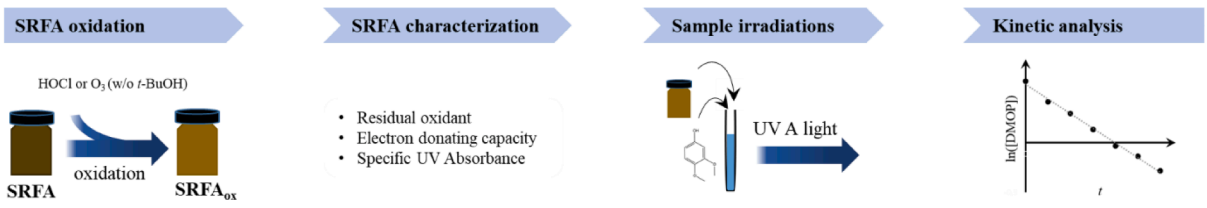

Fig. 1. Workflow for the photochemical experiments with pre-oxidized SRFA, including (i) SRFA oxidation, (ii) SRFA characterization by UV and EDC (relative to non-oxidized DOM), (iii) irradiation of sample and (iv) determination DMOP abatement kinetics.

320 nm. Dark experiments were performed for every SRFA batch with initial DMOP concentrations of 0.1 or 5.0 μM.

The photon fluence rate in the relevant wavelength range of 334−436 nm, E_p^*(334−436 nm), was measured weekly using the *para*-nitroanisol/pyridine actinometer and determined to be (5.0 ± 0.3) × 10^{-3} Einstein m^{-2} s^{-1} (details of the calculations are provided in the Supporting Information (SI), Text S1).

2.5. Analytical instrumentation

Concentrations of DMOP were determined using high-performance liquid chromatography (HPLC), utilizing an Agilent 1100 HPLC system, equipped with a quaternary low-pressure mixing gradient pump, a photodiode array detector, and a fluorescence detector (Agilent 1200 series). The photodiode array detector was used to analyze samples from solutions with an initial DMOP concentration of 5.0 μM (detection wavelength of 220 nm), whereas for samples for an initial DMOP concentration of 0.1 μM, the fluorescence detector was preferred as it reaches higher sensitivity (excitation/emission wavelength: 230/325 nm). Typically, duplicate injections of 50 μL samples were performed. A reverse-phase C_{18} column (COSMOSIL 5C18-MS-II packed column, pore size 120 Å, particle size 5 μm, internal diameter 3.0 mm, length 100 mm) with a column oven temperature of 25 °C was used. Using an isocratic method with an eluent consisting of 75% 10 mM aqueous phosphoric acid (pH 2.1) and 25% acetonitrile, and a flow rate of 0.5 mL min^{-1}, DMOP eluted with a retention time of 2.6 min. Standard deviations of duplicate measurements were typically < 5%.

The pH of the oxidized DOM solutions and of the sample solution prior and after the irradiation experiments were measured using a pH meter (Metrohm Model 605 equipped with a Metrohm pH electrode Model 6.02341.110). Generally, a small pH decrease (< 0.1 pH units) was observed during the irradiation experiments.

2.6. Kinetics of DOM-induced phototransformations

Pseudo-first-order rate constants for the phototransformation of DMOP were determined as the slope of linear regression lines for the natural logarithmic concentration values (ln[DMOP]) as a function of the irradiation time. The rate constants were denoted as $k_{0.1}^{obs}$ and $k_{5.0}^{obs}$ for initial DMOP concentrations of 0.1 and 5.0 μM, respectively. No correction of the DOM light screening effect was applied, since for the employed SRFA concentration (2.5 $mg_C L^{-1}$) such corrections (< 5%) (Remke et al., 2021) are smaller than the experimental error in k^{obs}.

The absorption properties of CDOM change as a consequence of oxidative treatment, which makes it important to analyze the efficiency of DMOP phototransformation in terms of absorbed photons. To this end, the rate constants $k_{0.1}^{obs}$ and $k_{5.0}^{obs}$ were scaled to r_{CDOM}^{abs}, the rate of light absorption by CDOM, and the corresponding ratios, $k_{0.1}^{obs}/r_{CDOM}^{abs}$ and $k_{5.0}^{obs}/r_{CDOM}^{abs}$, were obtained. r_{CDOM}^{abs} was calculated based on the photon fluence rate determined by chemical actinometry and the decadic absorption coefficient of the considered CDOM solutions (for calculation details, see SI, Text S2). By analogy to Eq. (1), $k_{5.0}^{obs}/r_{CDOM}^{abs}$ corresponds approximately to f_{DMOP}, the quantum yield coefficient for DMOP-transforming ^{3}CDOM*. The underlying assumption is that, at the initial DMOP concentration of 5 μM, the phototransformation of DMOP is almost exclusively due to reaction with ^{3}CDOM*. By contrast, for $k_{0.1}^{obs}/r_{CDOM}^{abs}$ there is no straightforward relationship to the formation quantum yield of LLPO, since the LLPO lifetime is not well defined and depends on the DMOP concentration. $k_{0.1}^{obs}/r_{CDOM}^{abs}$ is proposed to be positively correlated to LLPO formation efficiency and to LLPO lifetime.

As a measure to represent the DMOP transformation kinetics for low compared to high initial concentrations, the enhancement factor (*EF*) was calculated, as the ratio $k_{0.1}^{obs}/k_{5.0}^{obs}$, in analogy to a previous study (Remke et al., 2021).

Results and discussion

3.1. Changes in SRFA bulk parameters

Results of changes in UV absorbance parameters ($SUVA_{254}$, E2:E3) and EDC as a function of increasing specific oxidant doses are shown in Fig. 2.

Linear correlations were obtained for the changes in SRFA of $SUVA_{254}$, E2:E3 and EDC as a function of the specific oxidant doses, in accordance with previous studies, as indicated in Table 1 (Leresche et al., 2021; Remucal et al., 2020; Wan et al., 2021; Wenk et al., 2013a). The parameters of the linear regressions are provided in Table S5 (SI) and plotted data is in Tables S6 - S8. $SUVA_{254}$ decreases with increasing specific oxidant dose, with a somewhat more pronounced decrease for ozonated samples (with/ without *t*-BuOH) than for chlorinated samples (Fig. 2a, spectra are in SI, Fig. S1). E2:E3 increases with increasing specific chlorine and ozone (with *t*-BuOH) doses (attributed to a decrease in molecular weight, Fig. 2b). Such changes in E2:E3 can be attributed on the one hand to reactions of chlorine or ozone with, e.g., activated aromatic compounds, leading to ring opening and fragmentation and finally yielding lower molecular weight compounds (Gallard and von Gunten 2002b; Jiang et al., 2020; Ramseier and von Gunten 2009), and on the other hand to oxidation of conjugated systems (Remucal et al., 2020). For ozonation in the absence of *t*-BuOH, E2:E3 remains fairly stable, indicating small changes in molecular weight and conjugated systems. This is expected from a higher contribution of $^{\bullet}$OH, which leads to smaller changes in the structure of DOM due to a lower selectivity of this oxidant (Remucal et al., 2020). Fig. 2c shows relative EDC changes versus applied oxidant dose, with the strongest EDC decrease for chlorination, followed by ozonation with *t*-BuOH and ozonation without *t*-BuOH. The slopes of the linear regressions were (units: mol_C $mol_{oxidant}^{-1}$): −6.7 ± 0.8 for chlorination, −3.3 ± 0.5 for ozonation with *t*-BuOH and −2.3 ± 0.3 for ozonation without *t*-BuOH. This is in agreement with previous studies, in which it has been suggested that chlorination leads to chlorinated phenols, which likely exert a smaller electron donating capacity than phenols (Önnby et al., 2018; Wenk et al., 2013a) and Table 1. For direct ozone reactions, an oxidation of phenolic moieties also leads to abatement of EDC, whereas, in absence of *t*-BuOH, a smaller ozone exposure and involvement of $^{\bullet}$OH renders this process less efficient (Wenk et al., 2013b).

3.2. DMOP phototransformation in aqueous solutions of oxidized SRFA

Fig. 3 shows the trends in $k_{0.1}^{obs}$ and $k_{5.0}^{obs}$, with increasing specific chlorine or ozone doses (without and with *t*-BuOH) and the corresponding data is provided in SI, Tables S9–S11. In untreated SRFA, $k_{0.1}^{obs}$ was more than tenfold of $k_{5.0}^{obs}$ and this enhancement was ascribed to the contribution of long-lived photooxidants (LLPO) in $k_{0.1}^{obs}$, whereas ^{3}CDOM* activity is assumed to be mainly responsible for $k_{5.0}^{obs}$ (Remke et al., 2021).

Trends in $k_{0.1}^{obs}$ with increasing specific molar oxidant doses differ from the corresponding trends in $k_{5.0}^{obs}$ for all of the applied oxidants. For chlorinated SRFA, $k_{0.1}^{obs}$ decreases moderately, whereas $k_{5.0}^{obs}$ stays constant over the range of applied HOCl doses (Fig. 3a). Ozonation in presence of *t*-BuOH leads to a strong decrease of $k_{0.1}^{obs}$, whereas $k_{5.0}^{obs}$ initially plateaus up to a specific ozone dose of 0.1 $mol_{O_3} \times mol_C^{-1}$ and decreases for higher specific ozone doses to 50% of the initial value (Fig. 3b). For SRFA ozonated without *t*-BuOH, a non-steady trend was observed for $k_{0.1}^{obs}$, with an initial decrease, followed by an increase with a local maximum at a specific ozone dose of 0.1 $mol_{O_3} \times mol_C^{-1}$ and a further decrease (Fig. 3c). In contrast, $k_{5.0}^{obs}$ decreases continuously. The particular non-linear trend in $k_{0.1}^{obs}$ was verified carefully to exclude an artefact and its implications will be discussed in more detail in the section on the enhancement factor for oxidized SRFA.

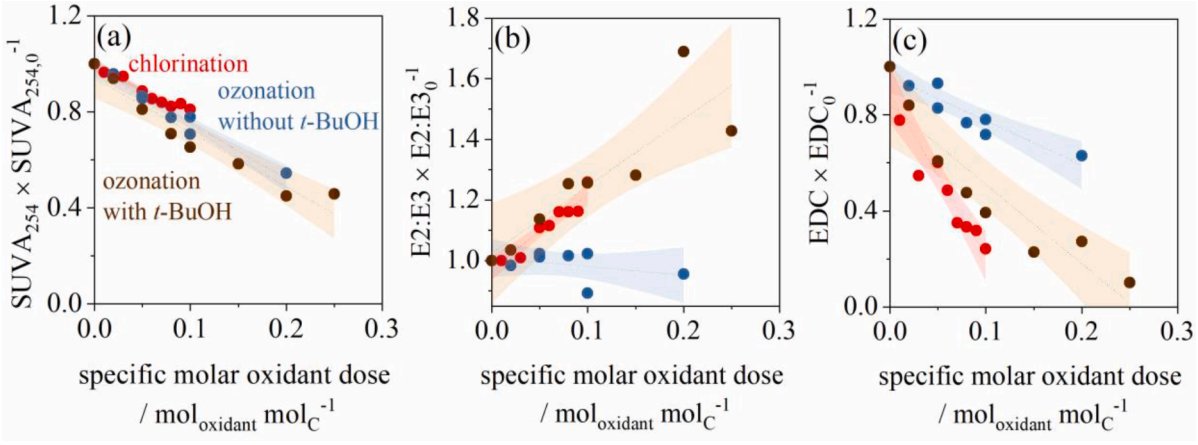

Fig. 2. Relative changes in bulk parameters for Suwannee River fulvic acid as a function of the specific molar oxidant dose with chlorine (red), ozone without *t*-BuOH (blue) and with *t*-BuOH (5 mM, brown): (a) Specific UV absorption coefficient at $\lambda = 254$ nm ($SUVA_{254}$), (b) ratio of specific UV absorbance at $\lambda = 254$ nm and $\lambda = 365$ nm, E2:E3 and (c) electron donating capacity (EDC). Dotted lines show the linear fit and transparent areas mark the area between the 95% confident bands as a guide for the eye. Oxidations were performed with aqueous SRFA solutions, 10 $mg_C L^{-1}$, pH 7, 10 mM phosphate buffer, at room temperature (23 ± 1 °C).

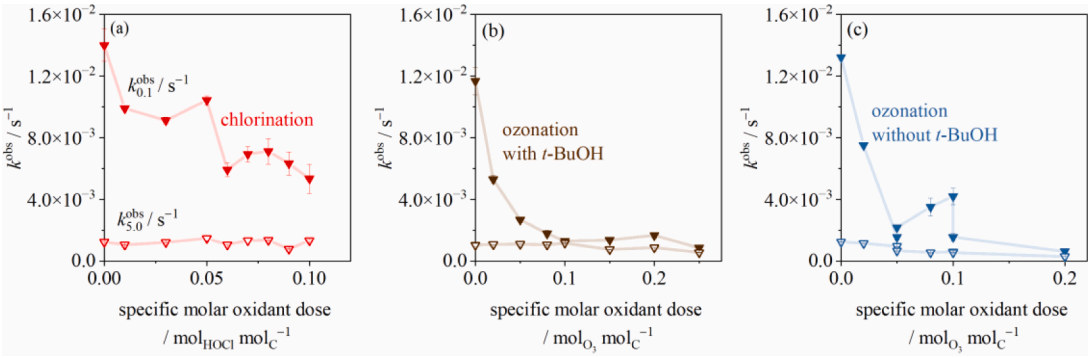

Fig. 3. Pseudo-first-order rate constants, $k_{0.1}^{obs}$ and $k_{5.0}^{obs}$, for phototransformation with 0.1 or 5.0 μM 3,4-dimethoxyphenol (DMOP), respectively, in aqueous solution containing non-oxidized or oxidized SRFA. SRFA was oxidized by (a) chlorine, (b) ozone with *t*-BuOH (5 mM), (c) ozone without *t*-BuOH with varying specific molar oxidant doses. Note the different scales in applied oxidant doses (*x*-axis). Oxidation experiments were performed with aqueous SRFA solutions, 10 $mg_C L^{-1}$, pH 7, 10 mM phosphate buffer, at room temperature (23 ± 1 °C), irradiation experiments were performed with diluted solutions, 2.5 $mg_C L^{-1}$, pH 8, 5 mM phosphate buffer, at 25 °C. Error bars (when not visible smaller than the symbols) indicate deviations of the mean for duplicate irradiation experiments.

These differences in trends between $k_{0.1}^{obs}$ and $k_{5.0}^{obs}$ corroborate the hypothesis of the involvement of different pools of SRFA moieties in DMOP phototransformation. In general, the photoactive functional groups contributing to $k_{0.1}^{obs}$ seem to be more affected by oxidation than for $k_{5.0}^{obs}$. Trends in $k_{5.0}^{obs}$ are in the expected range of changes for ^{3}CDOM*-induced compound phototransformation based on previous studies (Leresche et al., 2019). The following section will compare the changes in DMOP transformation kinetics with the changes in EDC and UV absorbance.

3.3. Correlation of DMOP phototransformation efficiency to changes in SRFA properties

In this sub-section, the photon absorption-based photochemical reactivity changes of pre-oxidized SRFA, $k_{0.1}^{obs}/r_{CDOM}^{abs}$ and $k_{5.0}^{obs}/r_{CDOM}^{abs}$, are considered in relation to specific oxidant doses and changes in $SUVA_{254}$, E2:E3 and EDC (Fig. 4).

As shown in Fig. 4, $k_{0.1}^{obs}/r_{CDOM}^{abs}$ decreases with increasing oxidant doses and the corresponding decrease in $SUVA_{254}$. It decreases moderately for chlorinated SRFA (~factor 2), and more strongly for ozonated SRFA (with and without *t*-BuOH) (~factor 3) for a 20% reduction in $SUVA_{254}$ compared to untreated SRFA (Fig. 4a, b). These decreasing trends indicate that a decrease in LLPO formation efficiency and/or lifetime is related to SRFA moieties that contribute to $SUVA_{254}$., i.e., aromatic moieties.

Moreover, $k_{0.1}^{obs}/r_{CDOM}^{abs}$ decreases strongly with increasing E2:E3 for ozonated SRFA (with *t*-BuOH) and moderately for chlorinated SRFA (Fig. 4c). In contrast, no clear trend of $k_{0.1}^{obs}/r_{CDOM}^{abs}$ versus E2:E3 can be observed for ozonated SRFA (without *t*-BuOH) (Fig. 4c). The trends for $k_{0.1}^{obs}/r_{CDOM}^{abs}$ versus E2:E3 differ between the oxidation methods, which suggests that LLPO formation does not strongly depend on DOM molecular weight and changes in conjugated systems.

$k_{0.1}^{obs}/r_{CDOM}^{abs}$ decreases with decreasing EDC for all three oxidation conditions (Fig. 4d). Even though EDC is less efficiently abated by ozone compared to chlorine (Fig. 2c), the effect of pre-ozonation on $k_{0.1}^{obs}/r_{CDOM}^{abs}$ is larger. Whereas ozone leads to e.g., benzoquinones, chlorination leads to chlorophenols (Acero et al., 2005; Gallard and von Gunten 2002a, b, Tentscher et al., 2018), which might still serve as LLPO precursors.

Analogous data for $k_{5.0}^{obs}/r_{CDOM}^{abs}$, which reflects the quantum yield coefficient f_{DMOP} for ^{3}CDOM*-induced DMOP transformation, are shown in Figs. 4e–h. f_{DMOP} increases with the specific molar oxidant dose for the SRFA treated by chlorination and ozonation with *t*-BuOH, whereas f_{DMOP} decreases for the ozonated SRFA in absence of *t*-BuOH (Fig. 4e). Also, f_{DMOP} increases with decreasing $SUVA_{254}$ and EDC, for chlorination and ozonation with *t*-BuOH (Fig. 4f, h). The observations of f_{DMOP} for chlorination and ozonation with *t*-BuOH are similar to the trends in

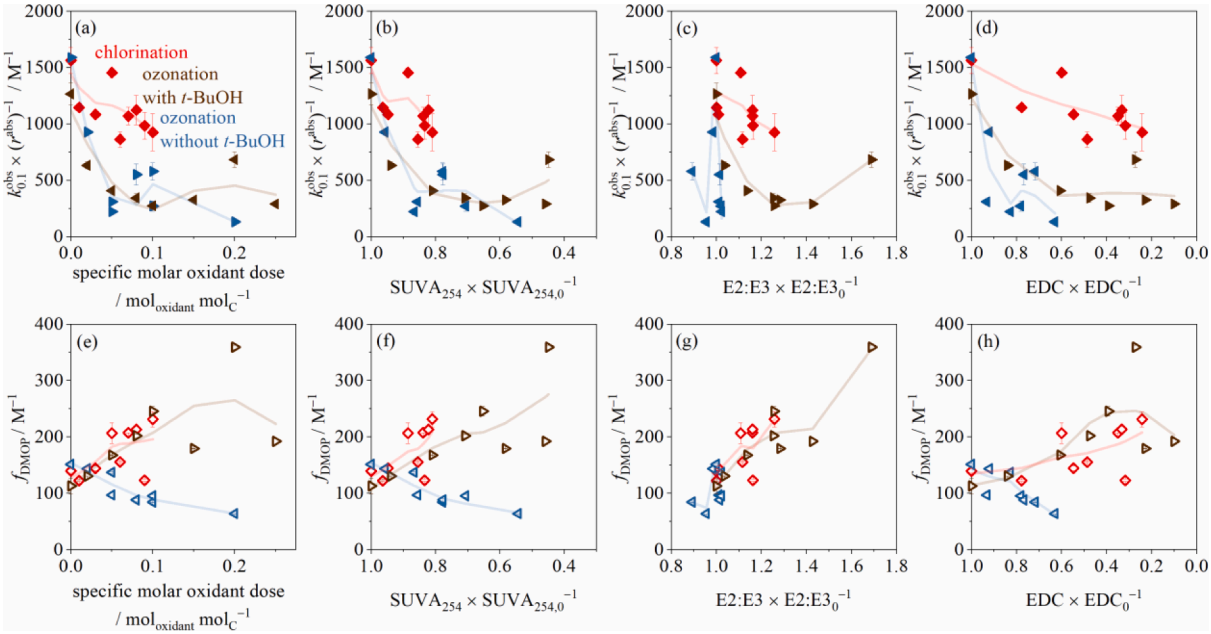

Fig. 4. Photon absorption-based 3,4-dimethoxyphenol (DMOP) phototransformation rate constants, (a–d) $k_{0.1}^{obs}/r_{CDOM}^{abs}$ and (e–h) $k_{5.0}^{obs}/r_{CDOM}^{abs} \approx f_{DMOP}$, for $[DMOP]_0$ = 0.1 and 5.0 μM, respectively, as a function of (a,e) the specific molar oxidant dose, (b, f) $SUVA_{254} \times SUVA_{254,0}^{-1}$, (c, g) $E2{:}E3 \times E2{:}E3_0^{-1}$, (d, h) $EDC \times EDC_0^{-1}$. Note the reverse scale of the *x*-axes in panels (b, f) and (d, h), which reflects the increase in oxidant dose from left to right; oxidations were performed as described in the captions of Fig. 3. Error bars (when not visible smaller than the symbols) indicate error propagations of deviations of the mean of duplicate irradiation experiments. The solid lines represent local polynomial regressions and are a guide for the eye.

^{3}CDOM* quantum yields which were observed in previous studies (Leresche et al., 2019; Leresche et al., 2021; Wan et al., 2021). In those studies, the increase in quantum yields with increasing oxidant dose, and observed decrease in $SUVA_{254}$ and EDC, was explained by the increase in ^{3}CDOM* precursors, such as quinones, formed during DOM oxidation (Önnby et al., 2018). For ozonation of SRFA without *t*-BuOH, the presence of $^{\bullet}$OH may lead to an abatement of ^{3}CDOM* precursors with a smaller formation of quinone-type moieties, which are more typically formed during ozone and chlorine reactions (Criquet et al., 2015; Ramseier and von Gunten 2009; Tentscher et al., 2018).

f_{DMOP} increases with increasing relative E2:E3 for all oxidation scenarios with an overall good linear fit (determination coefficient: 0.75) for f_{DMOP} with $E2{:}E3 \times E2{:}E3_0^{-1}$ (Fig. 4g, for linear fit see Fig. S3, SI). Also, f_{TMP}, is often positively correlated with E2:E3, and this correlation is rationalized by higher ^{3}CDOM* formation efficiencies by low molecular weight DOM moieties compared to high molecular weight DOM functional groups (Berg et al., 2019; Maizel and Remucal 2017; O'Connor et al., 2019; Trubetskaya et al., 2007).

Upon oxidation of SRFA, its photochemical activity changes, whereby the trends in $k_{0.1}^{obs}/r_{CDOM}^{abs}$ with increasing oxidant dose and the above-discussed CDOM bulk parameters (Figs. 4a–d) differ from those in f_{DMOP} (Figs. 4e–h). This observation is in line with the different nature of LLPO and ^{3}CDOM*, confirming that these photooxidants are related to different moieties of DOM.

3.4. Enhancement factor (EF) for oxidized SRFA

The *EF* was introduced in a previous study to assess the relative importance of LLPO on target compound transformation by factoring out the impact of ^{3}CDOM* (Remke et al., 2021). For *EF* = 1, LLPO only play a minor role for the transformation and they do not need to be included in the modeling of degradation kinetics of aquatic organic contaminants.

The general tendency is that *EF*, and therefore the importance of LLPO compared to ^{3}CDOM*, decreases with increasing oxidant dose, with a stronger decrease for ozonation (with/ without *t*-BuOH) compared to chlorination (Fig. 5a). However, the *EF* in ozonated samples without $^{\bullet}$OH scavenging (without *t*-BuOH) shows a second maximum at a specific oxidant dose of 0.1 mol O_3/mol C (Fig. 5a), with a continuous decrease in $SUVA_{254}$ and EDC (Fig. 5b, c). The behavior is not observed in the presence of an $^{\bullet}$OH scavenger, indicating an interplay of formation and abatement reactions with $^{\bullet}$OH. Such reactions with benzene structures within DOM might lead to deactivated phenols (e.g. methyl 4-hydroxybenzoate) which act as LLPO, thus lead to an enhancement, but are expected to exhibit comparatively weak EDC values. Interestingly, in the range of oxidant doses employed in this study, *EF* is significantly larger than unity, meaning that LLPO should be considered in modeling the degradation of contaminants that are comparably susceptible to LLPO as DMOP. LLPO precursors are suggested to be phenolic moieties, which are more reactive with the selected oxidants than the ^{3}CDOM* precursors, which likely contain aromatic ketone moieties (Canonica and Freiburghaus 2001; McNeill and Canonica 2016). At pH 7 the apparent second-order rate constant ($k_{obs,\ pH7}$) for the reaction of ozone with phenol is ~ (1.5 – 1.8) × 10^6 $M^{-1}s^{-1}$ (Hoigné and Bader 1983; Tentscher et al., 2018). For benzophenone, a model DOM sensitizer (McNeill and Canonica 2016) $k_{obs,\ pH7}$ is expected to be similar to the structurally analogous ketoprofen with *k* = 0.4 $M^{-1}s^{-1}$ (Real et al., 2009; von Sonntag and von Gunten 2012). For chlorine, the reaction with benzophenone or other aromatic ketones is expected to be very low (Deborde and von Gunten 2008).

4. Environmental implications

The aim of this study was to test the photoreactivity of pre-oxidized SRFA with different initial concentrations of 3,4-dimethoxyphenol (DMOP) employed as a probe compound and to evaluate the hypothesis that long-lived photooxidants (LLPO) consist of phenoxyl radicals. To test this, SRFA was oxidized by chlorination and ozonation (with/ without *t*-BuOH) and DMOP transformation was measured in aqueous solution of the pre-oxidized SRFA with two initial concentrations, namely 0.1 and 5.0 μM. Table 2 summarizes the observed trends in DOM absorbance, EDC and DOM-induced phototransformation kinetics for

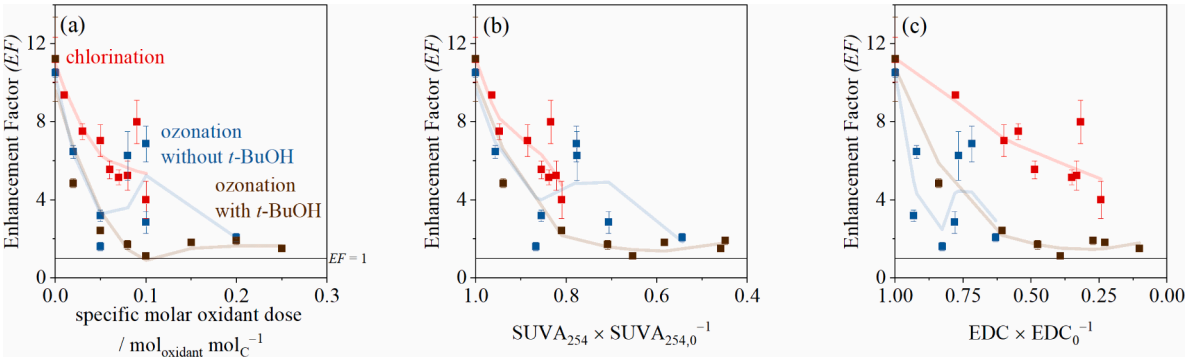

Fig. 5. Enhancement factor (ratio $k_{0.1}^{obs}$: $k_{5.0}^{obs}$) for DMOP transformation photosensitized by pre-oxidized SRFA with chlorine (red), ozone without *t*-BuOH (blue) and with *t*-BuOH (5 mM, brown) as a function of (a) the specific oxidant dose, (b) changes in relative $SUVA_{254}$ and (c) changes in relative EDC. Error bars (when not visible, smaller than the symbols) indicate error propagations of deviations of the mean of duplicate irradiation experiments. The solid lines represent local polynomial regression models to guide the eye.

Table 2
Relative and qualitative changes in $SUVA_{254}$, EDC, E2:E3 and photoreactivity induced by pre-oxidation of SRFA. Blue arrows indicate decrease, yellow arrows increase and the black arrow stagnation, size and intensity of the color indicate relative extent of the change.

	$SUVA_{254}$	EDC	E2:E3	$\frac{k_{0.1}^{obs}}{r_{CDOM}^{abs}}$	$\frac{k_{5.0}^{obs}}{r_{CDOM}^{abs}}$
Surrogate for	*Aromaticity*	*Phenol content*	*Molecular weight*	*LLPO formation efficiency & lifetime*	$\Phi_{^3CDOM^*}$
Chlorination	↓	↓	↑	↓	↑
Ozonation with *t*-BuOH	↓	↓	↑	↓	↑
Ozonation without *t*-BuOH	↓	↓	→	↓	↓

increasing specific oxidant doses. $SUVA_{254}$, EDC and normalized $k_{0.1}^{obs}$ decreased with increasing chlorine and ozone doses. E2:E3 and normalized $k_{5.0}^{obs}$ increased with increasing chlorine and ozone doses (with *t*-BuOH) and stagnated or slightly decreased with increasing ozone doses (without *t*-BuOH). These opposite trends in normalized $k_{0.1}^{obs}$ and $k_{5.0}^{obs}$ support the hypothesis of two different pools of photooxidants formed upon light absorption of DOM. Thereby, the precursors of the pool of long-lived photooxidants are affected by changes in DOM aromaticity and phenol content, but unaffected by changes in molecular weight or in conjugated systems. In contrast, precursors of the short-lived ^{3}CDOM* are affected by changes in DOM molecular weight.

5. Conclusions

In this study the fate of long-lived photooxidants was tested by oxidative treatment of phenolic DOM moieties. The photochemical reactivity of gradually oxidized SRFA was evaluated and compared to changes in $SUVA_{254}$, E2:E3 ratios and EDC. DMOP was employed as probe compound at initial concentrations of 0.1 and 5.0 μM. The transformation kinetics for an initial concentration of 0.1 μM was used as an indicator for the LLPO formation rate. Transformations at initial DMOP concentrations of 5.0 μM were used as an indicator for ^{3}CDOM* quantum yields.

The main outcomes of this study are:

- For the pre-oxidations of SRFA with chlorine or ozone, close to linear correlations were observed for the changes of $SUVA_{254}$, E2:E3 and EDC as a function of the oxidant doses, in line with previous studies. This relationship is a result of the reactions of chlorine and ozone with the oxidant- susceptible moieties in DOM such as phenols.
- For low initial DMOP concentrations, the pseudo-first-order transformation rate constant normalized for the changes in SRFA absorbance, decreased significantly for chlorinated and ozonated (with/without *t*-BuOH) SRFA, whereas for high initial DMOP concentrations, transformations were slightly enhanced for chlorinated and ozonated (with *t*-BuOH) and constant for ozonated SRFA (without *t*-BuOH). This contrasting observation corroborates the hypothesis of the formation of two distinct pools of photooxidants, differing in their lifetime and precursor moieties.
- For low initial DMOP concentrations, decreasing relative $SUVA_{254}$ and EDC correlate with a decrease in pseudo-first-order transformation rate constants. This hints to the involvement of phenolic moieties as photooxidant precursors. There was no clear trend for E2:E3 for the three pre-oxidation processes. Therefore, it can be hypothesized that LLPO formation is independent of the molecular weight and conjugated systems.
- For the higher initial DMOP concentrations, the quantum yield coefficient, f_{DMOP}, correlates with the relative changes in E2:E3. This is consistent with previous studies and can be interpreted as an increased ^{3}CDOM* formation from low molecular weight DOM.

- The enhancement factor, reflecting the impact of LLPO compared to ^{3}CDOM* on contaminant transformation, decreases with increasing oxidant doses and therefore decreasing $SUVA_{254}$ and EDC. Thus, LLPO precursors are more susceptible to oxidation than ^{3}CDOM* precursors supporting the hypothesis that LLPO consist of phenoxyl radicals, having DOM phenolic moieties as their precursors.

Funding

This study was supported by the Swiss National Science Foundation (Project No. 200021-169422).

Declaration of Competing Interest

The authors declare that they have no known competing financial interests or personal relationships that could have appeared to influence the work reported in this paper.

Data availability

Data will be made available on request.

Acknowledgments

The authors would like to thank Ursula Schönenberger and Elisabeth Muck for technical and laboratory support.

Supplementary materials

Supplementary material associated with this article is provided, in the online version, at doi:10.1016/j.watres.2023.119921.

References

Acero, J.L., Piriou, P., von Gunten, U., 2005. Kinetics and mechanisms of formation of bromophenols during drinking water chlorination: assessment of taste and odor development. Water Res. 39 (13), 2979–2993.
Aeschbacher, M., Graf, C., Schwarzenbach, R.P., Sander, M., 2012. Antioxidant properties of humic substances. Environ. Sci. Technol. 46 (9), 4916–4925.
APHA (2005) Standard methods for the examination of water and wastewater.
Berg, S.M., Whiting, Q.T., Herrli, J.A., Winkels, R., Wammer, K.H., Remucal, C.K., 2019. The role of dissolved organic matter composition in determining photochemical reactivity at the molecular level. Environ. Sci. Technol. 53 (20), 11725–11734.
Bodhipaksha, L.C., Sharpless, C.M., Chin, Y.P., Sander, M., Langston, W.K., MacKay, A. A., 2015. Triplet photochemistry of effluent and natural organic matter in whole water and isolates from effluent-receiving rivers. Environ. Sci. Technol. 49 (6), 3453–3463.
Buschmann, J., Canonica, S., Sigg, L., 2005. Photoinduced oxidation of antimony (III) in the presence of humic acid. Environ. Sci. Technol. 39 (14), 5335–5341.
Canonica, S., Freiburghaus, M., 2001. Electron-rich phenols for probing the photochemical reactivity of freshwaters. Environ. Sci. Technol. 35 (4), 690–695.
Canonica, S., Hoigné, J., 1995. Enhanced oxidation of methoxy phenols at micromolar concentration photosensitized by dissolved natural organic material. Chemosphere 30 (12), 2365–2374.
Criquet, J., Rodriguez, E.M., Allard, S., Wellauer, S., Salhi, E., Joll, C.A., von Gunten, U., 2015. Reaction of bromine and chlorine with phenolic compounds and natural organic matter extracts–Electrophilic aromatic substitution and oxidation. Water Res. 85, 476–486.
Deborde, M., von Gunten, U., 2008. Reactions of chlorine with inorganic and organic compounds during water treatment—Kinetics and mechanisms: a critical review. Water Res. 42 (1–2), 13–51.
Derrien, M., Brogi, S.R., Gonçalves-Araujo, R., 2019. Characterization of Aquatic Organic Matter: Assessment, Perspectives and Research Priorities, 163. Water Research, 114908. Article.
Gallard, H., von Gunten, U., 2002a. Chlorination of natural organic matter: kinetics of chlorination and of THM formation. Water Res. 36 (1), 65–74.
Gallard, H., von Gunten, U., 2002b. Chlorination of phenols: kinetics and formation of chloroform. Environ. Sci. Technol. 36 (5), 884–890.
Golanoski, K.S., Fang, S., Del Vecchio, R., Blough, N.V., 2012. Investigating the mechanism of phenol photooxidation by humic substances. Environ. Sci. Technol. 46 (7), 3912–3920.
Guo, Z., Kodikara, D., Albi, L.S., Hatano, Y., Chen, G., Yoshimura, C., Wang, J., 2022. Photodegradation of organic micropollutants in aquatic environment: importance, factors and processes. Water Res. 231, 118236.
Helms, J.R., Stubbins, A., Ritchie, J.D., Minor, E.C., Kieber, D.J., Mopper, K., 2008. Absorption spectral slopes and slope ratios as indicators of molecular weight, source, and photobleaching of chromophoric dissolved organic matter. Limnol. Oceanogr. 53 (3), 955–969.
Hoigné, J., Bader, H., 1980. Bestimmung von Ozon und Chlordioxid in Wasser mit der Indigo-Methode. Vom Wasser 55, 261–280.
Hoigné, J., Bader, H., 1983. Rate constants of reactions of ozone with organic and inorganic compounds in water—II: dissociating organic compounds. Water Res. 17 (2), 185–194.
Houska, J., Salhi, E., Walpen, N., von Gunten, U., 2021. Oxidant-reactive Carbonous Moieties in Dissolved Organic matter: Selective Quantification by Oxidative Titration Using Chlorine Dioxide and Ozone. Water Research (submitted).
Jiang, J., Han, J., Zhang, X., 2020. Nonhalogenated aromatic DBPs in drinking water chlorination: a gap between NOM and halogenated aromatic DBPs. Environ. Sci. Technol. 54 (3), 1646–1656.
Kawaguchi, H., 1993. Rates of sensitized photo-oxidation of 2,4,6-trimethylphenol by humic acid. Chemosphere 27 (11), 2177–2182.
Leenheer, J.A., Croué, J.P., 2003. Characterizing aquatic dissolved organic matter. Environ. Sci. Technol. 37 (1), 18A–26A.
Leresche, F., McKay, G., Kurtz, T., von Gunten, U., Canonica, S., Rosario-Ortiz, F.L., 2019. Effects of ozone on the photochemical and photophysical properties of dissolved organic matter. Environ. Sci. Technol. 53 (10), 5622–5632.
Leresche, F., Torres-Ruiz, J.A., Kurtz, T., von Gunten, U., Rosario-Ortiz, F.L., 2021. Optical properties and photochemical production of hydroxyl radical and singlet oxygen after ozonation of dissolved organic matter. Environ. Sci.: Water Res. Technol. 7 (2), 346–356.
Maizel, A.C., Remucal, C.K., 2017. Molecular composition and photochemical reactivity of size-fractionated dissolved organic matter. Environ. Sci. Technol. 51 (4), 2113–2123.
McNeill, K., Canonica, S., 2016. Triplet state dissolved organic matter in aquatic photochemistry: reaction mechanisms, substrate scope, and photophysical properties. Environ. Sci.: Process. Impacts 18 (11), 1381–1399.
Milstead, R.P., Remucal, C.K., 2021. Molecular-level insights into the formation of traditional and novel halogenated disinfection byproducts. ACS ES&T Water 1 (8), 1966–1974.
Mvula, E., von Sonntag, C., 2003. Ozonolysis of phenols in aqueous solution. Org. Biomol. Chem. 1 (10), 1749–1756.
O'Connor, M., Helal, S.R., Latch, D.E., Arnold, W.A., 2019. Quantifying photo-production of triplet excited states and singlet oxygen from effluent organic matter. Water Res. 156, 23–33.
Önnby, L., Salhi, E., McKay, G., Rosario-Ortiz, F.L., von Gunten, U., 2018. Ozone and chlorine reactions with dissolved organic matter-assessment of oxidant-reactive moieties by optical measurements and the electron donating capacities. Water Res. 144, 64–75.
Peuravuori, J., Pihlaja, K., 1997. Molecular size distribution and spectroscopic properties of aquatic humic substances. Anal. Chim. Acta 337 (2), 133–149.
Ramseier, M.K., von Gunten, U., 2009. Mechanisms of phenol ozonation — kinetics of formation of primary and secondary reaction products. Ozone: Sci. Eng. 31 (3), 201–215.
Real, F.J., Benitez, F.J., Acero, J.L., Sagasti, J.J., Casas, F., 2009. Kinetics of the chemical oxidation of the pharmaceuticals primidone, ketoprofen, and diatrizoate in ultrapure and natural waters. Ind. Eng. Chem. Res. 48 (7), 3380–3388.
Remke, S.C., Bürgin, T.H., Ludvíková, L., Heger, D., Wenger, O.S., von Gunten, U., Canonica, S., 2022. Photochemical oxidation of phenols and anilines mediated by phenoxyl radicals in aqueous solution. Water Res. 213, 118095.
Remke, S.C., von Gunten, U., Canonica, S., 2021. Enhanced transformation of aquatic organic compounds by long-lived photooxidants (LLPO) produced from dissolved organic matter. Water Res. 190, 116707. Article.
Remucal, C.K., Salhi, E., Walpen, N., von Gunten, U., 2020. Molecular-level transformation of dissolved organic matter during oxidation by ozone and hydroxyl radical. Environ. Sci. Technol. 54 (16), 10351–10360.
Richard, C., Canonica, S., 2005. In: Hutzinger, O. (Ed.), The Handbook of Environmental Chemistry, Vol 2. Springer, Berlin, Germany, pp. 299–323. Part M.
Rosario-Ortiz, F.L., Canonica, S., 2016. Probe compounds to assess the photochemical activity of dissolved organic matter. Environ. Sci. Technol. 50 (23), 12532–12547.
Sharpless, C.M., 2012. Lifetimes of triplet dissolved natural organic matter (DOM) and the effect of $NaBH_4$ reduction on singlet oxygen quantum yields: implications for DOM photophysics. Environ. Sci. Technol. 46 (8), 4466–4473.
Tentscher, P.R., Bourgin, M., von Gunten, U., 2018. Ozonation of *para*-substituted phenolic compounds yields *p*-benzoquinones, other cyclic α, β-unsaturated ketones, and substituted catechols. Environ. Sci. Technol. 52 (8), 4763–4773.
Trubetskaya, O., Trubetskoj, O., Richard, C., 2007. Photodegrading properties of soil humic acids fractionated by SEC-PAGE set-up. Are they connected with absorbance? J. Photochem. Photobiol. A: Chem. 189 (2–3), 247–252.
Vione, D., Minella, M., Maurino, V., Minero, C., 2014. Indirect photochemistry in sunlit surface waters: photoinduced production of reactive transient species. Chem. - A Eur. J. 20 (34), 10590–10606.
von Sonntag, C., von Gunten, U., 2012. Chemistry of Ozone in Water and Wastewater treatment: from Basic Principles to Applications. IWA Publishing.

Walpen, N., Houska, J., Salhi, E., Sander, M., von Gunten, U., 2020. Quantification of the electron donating capacity and UV absorbance of dissolved organic matter during ozonation of secondary wastewater effluent by an assay and an automated analyzer. Water Res. 185, 116235. Article.

Walpen, N., Schroth, M.H., Sander, M., 2016. Quantification of phenolic antioxidant moieties in dissolved organic matter by flow-injection analysis with electrochemical detection. Environ. Sci. Technol. 50 (12), 6423–6432.

Wan, D., Wang, H., Sharma, V.K., Selvinsimpson, S., Dai, H., Luo, F., Wang, C., Chen, Y., 2021. Mechanistic investigation of enhanced photoreactivity of dissolved organic matter after chlorination. Environ. Sci. Technol. 55 (13), 8937–8946.

Weishaar, J.L., Aiken, G.R., Bergamaschi, B.A., Fram, M.S., Fujii, R., Mopper, K., 2003. Evaluation of specific ultraviolet absorbance as an indicator of the chemical composition and reactivity of dissolved organic carbon. Environ. Sci. Technol. 37 (20), 4702–4708.

Wenk, J., Aeschbacher, M., Salhi, E., Canonica, S., von Gunten, U., Sander, M., 2013a. Chemical oxidation of dissolved organic matter by chlorine dioxide, chlorine, and ozone: effects on its optical and antioxidant properties. Environ. Sci. Technol. 47 (19), 11147–11156.

Wenk, J., Aeschbacher, M., Sander, M., von Gunten, U., Canonica, S., 2015. Photosensitizing and inhibitory effects of ozonated dissolved organic matter on triplet-induced contaminant transformation. Environ. Sci. Technol. 49 (14), 8541–8549.

Wenk, J., Eustis, S.N., McNeill, K., Canonica, S., 2013b. Quenching of excited triplet states by dissolved natural organic matter. Environ. Sci. Technol. 47 (22), 12802–12810.